Noname manuscri	ipt No.
(will be inserted by	the editor)

A thin double layer analysis of asymmetric rectified electric fields (AREFs)

Bhavya Balu · Aditya S. Khair

April 7, 2021

Abstract We use perturbation methods to analyze the "asymmetric rectified electric field (AREF)" generated when an oscillating voltage is applied across a model electrochemical cell consisting of a binary, asymmetric electrolyte bounded by planar, parallel, blocking electrodes. The AREF refers to the steady component of the electric potential gradient within the electrolyte, as discovered via numerics by Hashemi Amrei et. al. [Hashemi Amrei, S. M. H., Bukosky, S. C., Rader, S. P., Ristenpart, W. D., & Miller, G. H. (2018), Physical Review Letters, 121(18), 185504.]. We adopt the Poisson-Nernst-Planck framework for ion transport in dilute electrolytes, taking into account unequal ionic diffusivities. We consider the mathematically singular, and practically relevant, limit of thin Debye layers, $1/(\kappa L) = \epsilon \to 0$, where κ^{-1} is the Debye length, and L is the length of the half-cell. The dynamics of the electric potential and ionic strength in the "bulk" electrolyte (i.e., outside the Debye layers) are solved subject to effective boundary conditions obtained from consideration of the Debye scale transport. We specifically analyze the case when the applied voltage has a frequency comparable to the inverse bulk ion diffusion time scale, $\omega = \mathcal{O}(D_A/L^2)$, where $D_A = 2D_+D_-/(D_+ + D_-)$ is the ambipolar diffusivity, and D_{\pm} are the ionic diffusivities. In this regime, the AREF extends throughout the bulk of the cell, varying on a lengthscale proportional to $\sqrt{D_A/\omega}$, and has a magnitude of $\mathcal{O}(\epsilon^2 k_B T/(Le))$ to leading order in ϵ . Here, k_B is the Boltzmann constant, T is temperature, and e is the charge on a proton. We obtain an analytical approximation for the AREF at weak voltages, $V_0 \ll k_B T/e$, where V_0 is the amplitude of the voltage, for which the AREF is $\mathcal{O}(\epsilon^2 V_0^2 e/(k_B T L))$. Our asymptotic scheme is also used to calculate a numerical approximation to the AREF that is valid up to logarithmically large voltages, $V_0 = \mathcal{O}((k_BT/e)\ln(1/\epsilon))$. The existence of an AREF implies that a charged colloidal particle undergoes net electrophoretic motion under the applied oscillatory voltage. Additionally, a gradient in the bulk ionic strength, caused by the difference in ionic diffusivities, leads to rectified diffusiophoretic particle motion. Here, we predict the electrophoretic and diffusiophoretic velocities for a rigid, spherical, colloidal particle. The diffusiophoretic velocity is comparable in magnitude to the electrophoretic velocity, and can thus affect particle motion in an AREF significantly.

1 Introduction

Electrolytes under time-dependent voltages have applications in dielectric impedance spectroscopy [1–3]; generating fluid flow in microfluidic devices, [4–8]; desalination and de-ionization through porous membranes [9–11]; colloidal directed assembly [12–14]; and separation of particles and macromolecules through dielectrophoresis [15–18]. In these applications, the transport of charged ions under the applied voltage is used to drive fluid flow, particle motion, or separation processes. Ion transport in dilute solutions is governed by the Poisson-Nernst-Planck (PNP) equations that are coupled, nonlinear, partial differential equations describing the ionic species balances and electric potential in the electrolyte [19, 20]. Inclusion of fluid flow is achieved by coupling advective ionic fluxes in the PNP equations with the Stokes equations including a Coulomb body force.

A simple, yet instructive, model system to study electrolyte dynamics is an electrochemical cell containing a monovalent, binary electrolyte flanked by parallel, blocking electrodes [21]. Here, it is assumed that the ion transport is one dimensional, normal to the electrodes, and there is no fluid flow. When the cell is subject to an external voltage, the ions in the electrolyte move towards oppositely charged electrodes and form a diffuse layer of charge near each electrode, called the 'Debye layer,' that effectively screens the applied voltage from the bulk of the cell. The thickness of this layer

is characterized by the Debye length,

$$\kappa^{-1} = \sqrt{\frac{\varepsilon k_B T}{2n_{eq} e^2}},\tag{1}$$

where ε is the permittivity of the electrolyte, k_B is the Boltzmann constant, T is the temperature, n_{eq} is the uniform equilibrium ionic strength (i.e., in the absence of applied voltage), and e is the charge on a proton. For a monovalent electrolyte with an ionic strength of 1 mM, the Debye length $\kappa^{-1}\approx 10$ nm. Typical electrochemical cells have dimensions $L\approx 10-100\mu \text{m}$ [3, 5, 7, 13], hence, the product $\kappa L\gg 1$. Physically, this means that the applied voltage drops rapidly over a very short length scale compared to the cell width, leading to large potential and ion concentration gradients within the Debye layer. This poses challenges for numerically solving the PNP equations; for example, the time steps for numerical solution have to be suitably small to ensure stability. Further, a uniform grid cannot practically be used to simultaneously resolve the Debye layer and cover the entire solution domain; thus, mesh refinement is required [22]. However, the singular mathematical nature of the limit $1/(\kappa L)\to 0$ can be exploited by perturbation methods [21, 23–25]. Electrolyte dynamics are well understood in the limit of weak applied voltages, $V\ll k_BT/e$, where k_BT/e is the thermal voltage [21]. For reference, at a temperature of T=298 K, the thermal voltage ≈ 25 mV. Specifically, at weak voltages (formally, to first order in $Ve/(k_BT)$) the PNP equations can be linearized about the equilibrium state of the electrolyte to yield the "linear response" dynamics of the system. Going beyond the linear response regime is done either by calculating weakly nonlinear contributions [26, 27], by singular asymptotic analyses at $\kappa L\gg 1$ [21, 23–25], or by solving the PNP equations numerically [22, 28–30].

An assumption made in many theoretical analyses of this model problem is that of electrolyte symmetry; that is, the ions in the electrolyte have equal diffusivities and magnitudes of valences. A key result of this assumption is that during charging or discharging in the linear response regime, the ionic strength is uniform throughout the cell. Thus, any electric field gradient in the electrolyte is purely due to the local charge density in the Debye layers. The bulk behaves as an Ohmic resistor, wherein the potential is a harmonic function, and the neutral "salt" concentration, or ionic strength, is equal to its (uniform) equilibrium value. Note, bulk salt depletion can occur at larger voltages due to uptake of salt by the nonlinear capacitance of the Debye layers [21, 23]. However, in any real system, this assumption of symmetry may be questionable. For example, the ratio of the diffusivites of the anion and cation for NaCl (sodium chloride), $D_{-}/D_{+} = 1.523$. The salt that comes closest to perfect symmetry is perhaps KCl (potassium chloride), where $D_{-}/D_{+} = 1.038$. (The ratios are calculated from values of ionic diffusivities at infinite dilution as reported by [31].) As we will show below, a difference in diffusivities transiently perturbs the ionic strength in the bulk electrolyte away from its equilibrium value, which in turn drives a transient field gradient in the bulk. This transient "concentration polarization" arises even in the linear response regime. Practically, accounting for the asymmetry could alter predictions made for charging time scales; particle motion; or fluid flow in the electrolyte. A specific phenomena that arises due to unequal ionic diffusivities is the "asymmetric rectified electric field (AREF)," that was recently predicted by Hashemi Amrei et. al. [28]. They considered an asymmetric binary electrolyte subject to an ac voltage whose amplitude is larger than the thermal voltage, thus, the system is in the nonlinear regime. They numerically solved the PNP equations and discovered that a sinusoidal input voltage with zero time-average produces a steady, or "rectified," electric field in the electrolyte. They analyzed the case when the frequency of the applied voltage was comparable to the inverse of the ion diffusion time scale across the cell. In this regime, the AREF is "long ranged," that is, it extends much farther into the electrolyte than the Debye layer. In further work from this group, the AREF was used to explain the levitation of colloidal particles near an electrode [32], and electrolyte-dependent flow reversals in induced-charged electro-osmosis [33]. Finally, they demonstrated that an approximation to the AREF can be obtained from a perturbation expansion of the PNP equations to second order in a weak applied voltage: specifically, they obtained the solution to the second-order problem numerically [34].

Here, we analyze the PNP equations governing ion transport in this model electrochemical system for an asymmetric electrolyte (with unequal diffusivities but equal valances) under an ac voltage, employing singular perturbation methods to leverage the thin Debye layer limit. The characteristic length scale, or "range," of the AREF emerges from our analysis as $\sqrt{D_A/\omega}$, where $D_A=2D_+D_-/(D_++D_-)$ is the ambi-polar diffusivity of neutral salt. This has been predicted from the numerical solution of the AREF [22]. Our analysis specifically examines frequencies comparable to the inverse bulk ion diffusion time scale, as in Refs. [22, 28, 34]. We also briefly consider the limit when the applied frequency is comparable to the inverse RC time scale. An important implication of the AREF is that a charged particle would exhibit net motion under an ac voltage. This has been experimentally observed as electrolyte-dependent colloidal particle motion to specific positions in the bulk [35, 36]. In addition to the net electric field, however, we also demonstrate that the bulk transient concentration polarization can give rise to diffusiophoretic particle motion [37, 38]. Hence, the velocity of a charged particle under an AREF would include electrophoretic and diffusiophoretic contributions, in general. We develop our thin Debye layer approximation in Section 2; present our main results and discuss in Section 3; discuss the implications for particle motion in Section 4; and offer a conclusion in Section 5.

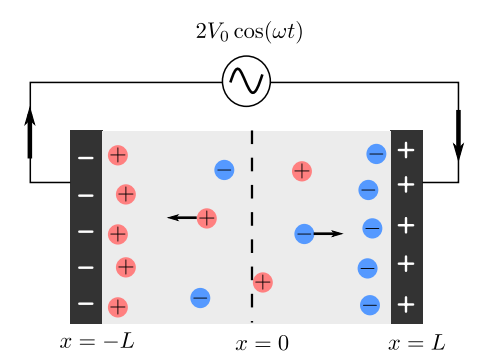


Fig. 1 Schematic of the model electrochemical cell consisting of a dilute asymmetric, monovalent, binary electrolyte between planar, blocking electrodes. The cell is subject to an ac voltage $2V_0 \cos(\omega t)$.

2 Problem formulation

Consider an electrochemical cell with planar, parallel, blocking, initially uncharged electrodes, containing a dilute, monovalent, binary electrolyte solution (Fig.1). The ions in the electrolyte have unequal diffusivities, $D_+ \neq D_-$. The cell is subject to a voltage $2V(t) = 2V_0\cos(\omega t)$, applied as $\pm V(t)$ to the right and left electrodes respectively. Here V_0 is the amplitude of the voltage signal, ω is its angular frequency, and t represents time. We assume that the dimensions of the electrodes are much larger than the spacing between them; thus, the PNP equations are one dimensional, with ion transport solely along the direction of the normal to the electrodes. Hence, there is no fluid flow in the system; the variation in local charge density is balanced by a dynamic pressure gradient [39]. The dimensionless PNP equations are

$$\frac{L^2 \omega}{D_{\pm}} \frac{\partial \tilde{n}_{\pm}}{\partial \tilde{t}} = \frac{\partial^2 \tilde{n}_{\pm}}{\partial \tilde{x}^2} \pm \frac{\partial}{\partial \tilde{x}} \left(\tilde{n}_{\pm} \frac{\partial \tilde{\phi}}{\partial \tilde{x}} \right), \quad \text{and} \quad \frac{\partial^2 \tilde{\phi}}{\partial \tilde{x}^2} = -\frac{1}{2} \left(\kappa L \right)^2 \left(\tilde{n}_{+} - \tilde{n}_{-} \right). \tag{2}$$

Here, \tilde{n}_{\pm} are the ion concentrations of the positive and negative ions normalized by the equilibrium ionic strength n_{eq} ; $\tilde{\phi}$ is the electric potential normalized by the thermal voltage k_BT/e ; \tilde{x} is the position normalized by the length of the half cell L; and \tilde{t} is time normalized by the inverse frequency ω^{-1} . In (2), the first equation describes the transport of ions under diffusion and electro-migration, and the second is Poisson's equation relating the field gradient to the local ionic space charge density. The tilde notation $\tilde{(\cdot)}$ is used to denote dimensionless variables. The system is subject to the following boundary conditions at the electrodes ($\tilde{x}=\pm 1$):

$$\frac{\partial \tilde{n}_{\pm}}{\partial \tilde{x}} \pm \tilde{n}_{\pm} \frac{\partial \tilde{\phi}}{\partial \tilde{x}} = 0, \quad \text{and} \quad \tilde{\phi} = \pm \tilde{V}(\tilde{t}), \tag{3}$$

which correspond to conditions of zero flux through the blocking electrodes, and the applied potential difference. It is useful to reformulate the governing equations in terms of the dimensionless ionic strength and the charge density, i.e., the sum and difference of the dimensionless ionic species concentrations. The dimensionless (mean) ionic strength and charge density are thus, $2\tilde{c}=(\tilde{n}_++\tilde{n}_-)$ and $2\tilde{\rho}=(\tilde{n}_+-\tilde{n}_-)$. This introduces the dimensionless frequencies $L^2\omega/D_A$ and $L^2\omega/D_F$ as important parameters where $D_A=2D_+D_-/(D_++D_-)$ is the ambipolar diffusivity of the salt, and $D_F=2D_+D_-/(D_--D_+)$. We define $\alpha=L^2\omega/D_A$, and $\beta=D_A/D_F=(D_--D_+)/(D_-+D_+)$. Note that when $D_+=D_-$, we have $\beta=0$. The PNP equations in terms of the ionic strength and charge density are

$$\alpha \frac{\partial \tilde{c}}{\partial \tilde{t}} + \alpha \beta \frac{\partial \tilde{\rho}}{\partial \tilde{t}} = \frac{\partial^2 \tilde{c}}{\partial \tilde{x}^2} + \frac{\partial}{\partial \tilde{x}} \left(\tilde{\rho} \frac{\partial \tilde{\phi}}{\partial \tilde{x}} \right), \tag{4}$$

$$\alpha\beta \frac{\partial \tilde{c}}{\partial \tilde{t}} + \alpha \frac{\partial \tilde{\rho}}{\partial \tilde{t}} = \frac{\partial^2 \tilde{\rho}}{\partial \tilde{x}^2} + \frac{\partial}{\partial \tilde{x}} \left(\tilde{c} \frac{\partial \tilde{\phi}}{\partial \tilde{x}} \right), \tag{5}$$

and

$$\frac{\partial^2 \tilde{\phi}}{\partial \tilde{x}^2} = -\left(\kappa L\right)^2 \tilde{\rho}.\tag{6}$$

The flux boundary conditions at $\tilde{x} = \pm 1$ then become

$$\frac{\partial \tilde{\rho}}{\partial \tilde{x}} + \tilde{c} \frac{\partial \tilde{\phi}}{\partial \tilde{x}} = 0, \quad \text{and} \quad \frac{\partial \tilde{c}}{\partial \tilde{x}} + \tilde{\rho} \frac{\partial \tilde{\phi}}{\partial \tilde{x}} = 0. \tag{7}$$

Hence, we have a system of coupled nonlinear partial differential equations (4) - (7) for $\tilde{\rho}$, \tilde{c} , and $\tilde{\phi}$, which would, in general, require numerical solution. Such solutions are challenging due to the typical scale disparity between the Debye length and the cell width, $\kappa L \gg 1$. Here, we are interested in the long-time oscillatory response, that is, after the initial transients have died out.

2.1 Thin Debye layer limit

To proceed, we seek asymptotic approximations that exploit the fact that $\kappa L \gg 1$. That is, we consider the limit $\epsilon \equiv 1/(\kappa L) \to 0$. It is readily seen that this limit is singular, as taking $\epsilon = 0$ leads to a reduction in the order of the Poisson equation (6). In this limit, we have two spatial regions: the bulk electrolyte, which is a distance of $\tilde{x} = \mathcal{O}(1)$ away from each electrode; and the Debye layers at each electrode, of thickness $\mathcal{O}(\epsilon)$. The leading order bulk dynamics can be found simply by setting $\epsilon \equiv 0$ in the PNP equations, the first consequence of which is $\tilde{\rho} = 0$, i.e., the bulk is electro-neutral to leading order; and then from (4) and (5),

$$\alpha \frac{\partial \tilde{c}}{\partial \tilde{t}} = \frac{\partial^2 \tilde{c}}{\partial \tilde{x}^2}, \quad \text{and} \quad \alpha \beta \frac{\partial \tilde{c}}{\partial \tilde{t}} = \frac{\partial}{\partial \tilde{x}} \left(\tilde{c} \frac{\partial \tilde{\phi}}{\partial \tilde{x}} \right).$$
 (8)

Unequal diffusivites implies $\beta \neq 0$; thus, the time variation of the bulk ionic strength drives a bulk field gradient. This would not happen if the diffusivities were equal. Now, $\tilde{\rho}$, \tilde{c} , and $\tilde{\phi}$ represent the leading order charge density, ionic strength, and electric potential in the bulk, in an asymptotic expansion as $\epsilon \to 0$.

We seek separate solutions that are valid inside the Debye layers. Consider the right electrode at $\tilde{x}=1$. We introduce an "inner" coordinate for the Debye layer near this electrode, defined as

$$\tilde{X} = \frac{\tilde{x} - 1}{\epsilon} = \mathcal{O}(1) \quad \text{as} \quad \epsilon \to 0.$$
 (9)

Thus, at the electrode surface, $\tilde{x}=1$, and $\tilde{X}=0$. In the bulk outside the Debye layer, $|\tilde{x}-1|\gg\epsilon$, and $\tilde{x}<1$, thus $\tilde{X}\to-\infty$. Now the Poisson equation inside the Debye layer becomes

$$\frac{\partial^2 \tilde{\Phi}}{\partial \tilde{X}^2} = -\tilde{P}.\tag{10}$$

The corresponding species balances are

$$\epsilon^2 \alpha \left[\frac{\partial \tilde{C}}{\partial \tilde{t}} + \beta \frac{\partial \tilde{P}}{\partial \tilde{t}} \right] = \frac{\partial^2 \tilde{C}}{\partial \tilde{X}^2} + \frac{\partial}{\partial \tilde{X}} \left(\tilde{P} \frac{\partial \tilde{\Phi}}{\partial \tilde{X}} \right), \tag{11}$$

$$\epsilon^2 \alpha \left[\beta \frac{\partial \tilde{C}}{\partial \tilde{t}} + \frac{\partial \tilde{P}}{\partial \tilde{t}} \right] = \frac{\partial^2 \tilde{P}}{\partial \tilde{X}^2} + \frac{\partial}{\partial \tilde{X}} \left(\tilde{C} \frac{\partial \tilde{\Phi}}{\partial \tilde{X}} \right). \tag{12}$$

Here the capital symbols \tilde{C} , \tilde{P} , and $\tilde{\Phi}$ represent the leading order ionic strength, charge density, and potential within the Debye layer, respectively. Next, we assume $\epsilon^2 \alpha \ll 1$, or equivalently, $\omega \ll \kappa^2 D_A$, that is, the frequency of oscillations is smaller than the inverse Debye relaxation time. Physically, this implies that the Debye layer charges quasi-steadily over each oscillation cycle. This is the only restriction we make on the frequency at this stage. Later, we consider separately the behavior of our system at two different scales of the applied frequency: Sec. 2.3 briefly considers when the frequency is on the order of the inverse of the RC time constant of the cell; and Sec. 2.4 describes in detail the case when the frequency is on the order of the inverse bulk diffusion time scale. The species balances imply

$$0 = \frac{\partial^2 \tilde{N}_+}{\partial \tilde{X}^2} + \frac{\partial}{\partial \tilde{X}} \left(\tilde{N}_+ \frac{\partial \tilde{\Phi}}{\partial \tilde{X}} \right), \quad \text{and} \quad 0 = \frac{\partial^2 \tilde{N}_-}{\partial \tilde{X}^2} - \frac{\partial}{\partial \tilde{X}} \left(\tilde{N}_- \frac{\partial \tilde{\Phi}}{\partial \tilde{X}} \right). \tag{13}$$

Here \tilde{N}_{\pm} are the concentrations of the positive and negative ions inside the Debye layers. Thus we find the ion concentrations in the Debye layer have a quasi-equilibrium Boltzmann profile,

$$\tilde{N}_{\pm} = \tilde{n}_{\pm} \exp\left[\pm(\tilde{\phi} - \tilde{\Phi})\right]. \tag{14}$$

Here \tilde{n}_{\pm} and $\tilde{\phi}$ are the bulk values as $\tilde{x} \to 1$. Further, the concentrations of the positive and negative ions in the bulk are equal, since the bulk is electro-neutral to leading order. Thus, $\tilde{n}_{+} = \tilde{n}_{-} = \frac{\tilde{c}}{2}$. Using (14) in the Poisson equation (10), we have that the potential in the Debye layer satisfies the Poisson-Boltzmann equation

$$\frac{\partial^2 \tilde{\Phi}}{\partial \tilde{X}^2} = \tilde{c} \sinh(\tilde{\Phi} - \tilde{\phi}),\tag{15}$$

which is subject to the boundary condition $\tilde{\Phi} = \tilde{V}(\tilde{t})$ at $\tilde{X} = 0$. Equation (15) can be integrated twice, using $\partial \tilde{\Phi}/\partial \tilde{X} = 0$ and $\tilde{\Phi} = \tilde{\phi}$ as $\tilde{X} \to -\infty$ (to match the bulk solution) to obtain

$$\tilde{\Phi} - \tilde{\phi} = 4 \tanh^{-1} \left[e^{\sqrt{\tilde{c}}\tilde{X}} \tanh\left(\frac{\tilde{\zeta}_r}{4}\right) \right], \tag{16}$$

where $\tilde{\zeta_r} = \tilde{\Phi}(0) - \tilde{\phi} = \tilde{V}(\tilde{t}) - \tilde{\phi}$ is the leading order zeta potential of the right electrode (at $\tilde{x} = 1$); that is, the net potential drop across the Debye layer. Note, (16) has been derived previously in various contexts, e.g., see Refs. [40–42].

2.2 Effective boundary conditions for the bulk solution

We connect the double layer and the bulk through effective boundary conditions for the bulk fields \tilde{c} and $\tilde{\phi}$ to be applied at $\tilde{x}=1$. To do this, we define dimensionless surface excess concentrations of the cations and anions near the electrode (in this case, at $\tilde{x}=1$) [23, 43]. The excess concentration in the Debye layer is with respect to the bulk value. This is integrated over the thickness of the Debye layer to obtain the surface excess concentration,

$$\tilde{\Gamma}_{\pm} = \epsilon \int_{-\infty}^{0} (\tilde{N}_{\pm} - \tilde{c}) d\tilde{X} = 2\epsilon \sqrt{\tilde{c}} \left(\exp(\mp \tilde{\zeta}_r/2) - 1 \right)$$
(17)

We use that the net flux of ions from the bulk into the Debye layers is balanced by the accumulation of surface excess concentration at each electrode. (Note that the surface excess concentration is normalized by $n_{eq}L$.) In our one dimensional system, this is written as

$$\frac{L^2 \omega}{D_+} \frac{\partial \tilde{\Gamma}_+}{\partial \tilde{t}} = -\left(\frac{\partial \tilde{n}_+}{\partial \tilde{x}} + \tilde{n}_+ \frac{\partial \tilde{\phi}}{\partial \tilde{x}}\right) \quad \text{at} \quad \tilde{x} = 1, \tag{18}$$

$$\frac{L^2 \omega}{D_-} \frac{\partial \tilde{\Gamma}_-}{\partial \tilde{t}} = -\left(\frac{\partial \tilde{n}_-}{\partial \tilde{x}} - \tilde{n}_- \frac{\partial \tilde{\phi}}{\partial \tilde{x}}\right) \quad \text{at} \quad \tilde{x} = 1.$$
 (19)

We relate the surface excess concentrations to the surface excess ionic strength \tilde{I}_r and charge density \tilde{R}_r in the Debye layer at $\tilde{x}=1$ as

$$\epsilon \tilde{I}_r = \frac{1}{2} \left(\tilde{\Gamma}_+ + \tilde{\Gamma}_- \right) \quad \text{and} \quad \epsilon \tilde{R}_r = \frac{1}{2} \left(\tilde{\Gamma}_+ - \tilde{\Gamma}_- \right).$$
 (20)

Using (17), we have

$$\tilde{I}_r = 4\sqrt{\tilde{c}} \left[\sinh^2(\tilde{\zeta}_r/4) \right] \quad \text{and} \quad \tilde{R}_r = -2\sqrt{\tilde{c}} \left[\sinh(\tilde{\zeta}_r/2) \right].$$
 (21)

The boundary conditions (18) and (19) are then added and subtracted to obtain

$$\alpha \epsilon \left[\frac{\partial \tilde{I}_r}{\partial \tilde{t}} + \beta \frac{\partial \tilde{R}_r}{\partial \tilde{t}} \right] = -\frac{\partial \tilde{c}}{\partial \tilde{x}}, \quad \text{and} \quad \alpha \epsilon \left[\beta \frac{\partial \tilde{I}_r}{\partial \tilde{t}} + \frac{\partial \tilde{R}_r}{\partial \tilde{t}} \right] = -\tilde{c} \frac{\partial \tilde{\phi}}{\partial \tilde{x}}, \quad \text{at} \quad \tilde{x} = 1.$$
 (22)

Thus, (22) represents the required effective boundary conditions on the ionic strength and potential at $\tilde{x}=1$. We have an equivalent analysis of the left electrode at $\tilde{x}=-1$ where the zeta potential is now $\tilde{\zeta}_l=-\tilde{V}(t)-\tilde{\phi}$. The surface excess ionic strength and charge density at the left electrode are

$$\tilde{I}_l = 4\sqrt{\tilde{c}} \left[\sinh^2(\tilde{\zeta}_l/4) \right] \quad \text{and} \quad \tilde{R}_l = -2\sqrt{\tilde{c}} \left[\sinh(\tilde{\zeta}_l/2) \right],$$
 (23)

and the effective boundary conditions on the left electrode are

$$\alpha \epsilon \left[\frac{\partial \tilde{I}_l}{\partial \tilde{t}} + \beta \frac{\partial \tilde{R}_l}{\partial \tilde{t}} \right] = \frac{\partial \tilde{c}}{\partial \tilde{x}}, \quad \text{and} \quad \alpha \epsilon \left[\beta \frac{\partial \tilde{I}_l}{\partial \tilde{t}} + \frac{\partial \tilde{R}_l}{\partial \tilde{t}} \right] = \tilde{c} \frac{\partial \tilde{\phi}}{\partial \tilde{x}}, \quad \text{at} \quad \tilde{x} = -1.$$
 (24)

Thus, the equations (8) along with (22) and (24), provide a macro-scale model of the bulk electrolyte, where the Debye-scale transport is encoded in the effective boundary conditions. The small parameter ϵ appears in these boundary conditions because we have normalized time with the inverse of the applied frequency, rather than choosing a time scale associated with diffusive ion transport.

2.3 Analysis at the RC frequency

A natural regime to consider is when the frequency is on the order of the inverse RC charging time [21], $\omega = \mathcal{O}(D_A/(\kappa^{-1}L))$ in dimensional variables, corresponding to $\alpha = \mathcal{O}(1/\epsilon)$. Here, one can 'gear' the frequency and dimensionless Debye length by defining $\sigma = \alpha \epsilon = \mathcal{O}(1)$ as $\epsilon \to 0$. Thus, ϵ disappears from the effective boundary conditions, (22) and (24), and instead enters the governing equations, (8). This prompts expansions for the bulk ionic strength and potential in orders of ϵ . The governing equations at leading order will then stipulate that the bulk ionic strength is uniform, which is incompatible with the dynamic effective boundary conditions. This mismatch points to the existence of a second, nested boundary layer that bridges the Debye layer and the bulk, the so-called the "diffusion layer," as has been elucidated for symmetric electrolytes beyond the linear-response, or weak voltage, regime [23]. The diffusion layer is also seen in problems involving transiently forced Debye layers, including polarization impedance of an electrode [44]; polarization of particles under ac fields [45]; and ac electroosmosis [46, 47]. The diffusion layers extend for a distance of $\mathcal{O}(\sqrt{\epsilon})$ from each electrode, and the variations in ionic strength and potential in the diffusion layers follow an expansion in orders of $\sqrt{\epsilon}$. Notably, in this limit, the leading order dynamics, and hence the AREF, are constrained to the diffusion layers; they do not extend throughout the cell. Hence, we do not pursue this analysis further.

2.4 Analysis at the bulk diffusion frequency

Here, we analyze the case when the frequency is on the order of the bulk diffusion time, $\omega = \mathcal{O}(D_A/L^2)$ in dimensional variables, corresponding to $\alpha = \mathcal{O}(1)$. This is relevant to the numerical computations of Hashemi Amrei et al. [22, 28, 34]. We pose the regular expansions for the bulk variables

$$\tilde{g} = \tilde{g}^{(0)} + \epsilon \tilde{g}^{(1)} + \epsilon^2 \tilde{g}^{(2)} + \mathcal{O}(\epsilon^2), \tag{25}$$

where \tilde{g} is \tilde{c} or $\tilde{\phi}$; and $\tilde{g}^{(0)}$, $\tilde{g}^{(1)}$, and $\tilde{g}^{(2)}$ are functions that are independent of ϵ . The leading order balances are, from (8)

$$\alpha \frac{\partial \tilde{c}^{(0)}}{\partial \tilde{t}} = \frac{\partial^2 \tilde{c}^{(0)}}{\partial \tilde{x}^2}, \quad \text{and} \quad \alpha \beta \frac{\partial \tilde{c}^{(0)}}{\partial \tilde{t}} = \frac{\partial}{\partial \tilde{x}} \left(\tilde{c}^{(0)} \frac{\partial \tilde{\phi}^{(0)}}{\partial \tilde{x}} \right). \tag{26}$$

From (22) and (24), the leading order boundary conditions at $\tilde{x} = \pm 1$ become

$$0 = \frac{\partial \tilde{c}^{(0)}}{\partial \tilde{x}}, \quad \text{and} \quad 0 = \tilde{c}^{(0)} \frac{\partial \tilde{\phi}^{(0)}}{\partial \tilde{x}}. \tag{27}$$

Thus the bulk ionic strength $\tilde{c}^{(0)}$ is a constant. We further get that $\tilde{c}^{(0)}=1$ from the requirement that the total number of ions must be conserved across the cell due to the blocking nature of the electrodes. Note, this result assumes that the net ion uptake by the $\mathcal{O}(\epsilon)$ wide Debye layers is o(1), and we will return to this issue below. The potential $\tilde{\phi}^{(0)}=0$; that is, there is no bulk electric field at leading order in ϵ . The leading order zeta potentials at the left and right electrode are thus $\tilde{\zeta}_l^{(0)}=-\tilde{V}(\tilde{t})$ and $\tilde{\zeta}_r^{(0)}=\tilde{V}(\tilde{t})$. Furthermore, since $\tilde{\phi}^{(0)}=0$ we see from Poisson's equation that the leading order charge density in the bulk is $o(\epsilon^2)$. This completes the leading order solution. Physically, at leading order the Debye layers are able to completely charge in a quasi-steady manner; thus, the applied potential is dropped entirely across these layers. Since bulk dynamics are absent at leading order, we seek the $\mathcal{O}(\epsilon)$ solutions. We have from (8)

$$\alpha \frac{\partial \tilde{c}^{(1)}}{\partial \tilde{t}} = \frac{\partial^2 \tilde{c}^{(1)}}{\partial \tilde{x}^2}, \quad \alpha \beta \frac{\partial \tilde{c}^{(1)}}{\partial \tilde{t}} = \frac{\partial^2 \tilde{\phi}^{(1)}}{\partial \tilde{x}^2}.$$
 (28)

These are subject to the boundary conditions, from (22),

$$\alpha \left[\frac{\partial \tilde{I}_{r}^{(0)}}{\partial \tilde{t}} + \beta \frac{\partial \tilde{R}_{r}^{(0)}}{\partial \tilde{t}} \right] = -\frac{\partial \tilde{c}^{(1)}}{\partial \tilde{x}}, \quad \text{and} \quad \alpha \left[\beta \frac{\partial \tilde{I}_{r}^{(0)}}{\partial \tilde{t}} + \frac{\partial \tilde{R}_{r}^{(0)}}{\partial \tilde{t}} \right] = -\frac{\partial \tilde{\phi}^{(1)}}{\partial \tilde{x}}, \quad \text{at} \quad \tilde{x} = 1; \tag{29}$$

and from (24),

$$\alpha \left[\frac{\partial \tilde{I}_{l}^{(0)}}{\partial \tilde{t}} + \beta \frac{\partial \tilde{R}_{l}^{(0)}}{\partial \tilde{t}} \right] = \frac{\partial \tilde{c}^{(1)}}{\partial \tilde{x}}, \quad \text{and} \quad \alpha \left[\beta \frac{\partial \tilde{I}_{l}^{(0)}}{\partial \tilde{t}} + \frac{\partial \tilde{R}_{l}^{(0)}}{\partial \tilde{t}} \right] = \frac{\partial \tilde{\phi}^{(1)}}{\partial \tilde{x}}, \quad \text{at} \quad \tilde{x} = -1. \tag{30}$$

Here, from (21),

$$\tilde{I}_r^{(0)} = 4 \sinh^2\left(\frac{\tilde{V}(\tilde{t})}{4}\right), \quad \text{and} \quad \tilde{R}_r^{(0)} = -2 \sinh\left(\frac{\tilde{V}(\tilde{t})}{2}\right);$$
 (31)

and from (23),

$$\tilde{I}_l^{(0)} = 4 \sinh^2 \left(\frac{\tilde{V}(\tilde{t})}{4} \right), \quad \text{and} \quad \tilde{R}_l^{(0)} = 2 \sinh \left(\frac{\tilde{V}(\tilde{t})}{2} \right). \tag{32}$$

Consider the right electrode, $\tilde{x} = 1$. Here, the time derivatives are

$$\frac{\partial \tilde{I}_{r}^{(0)}}{\partial \tilde{t}} = \sinh\left(\frac{\tilde{V}(\tilde{t})}{2}\right) \frac{d\tilde{V}(\tilde{t})}{d\tilde{t}} \quad \text{and} \quad \frac{\partial \tilde{R}_{r}^{(0)}}{\partial \tilde{t}} = -\cosh\left(\frac{\tilde{V}(\tilde{t})}{2}\right) \frac{d\tilde{V}(\tilde{t})}{d\tilde{t}}. \tag{33}$$

The effective boundary conditions are thus, at $\tilde{x} = 1$,

$$\alpha \left[\sinh \left(\frac{\tilde{V}(\tilde{t})}{2} \right) - \beta \cosh \left(\frac{\tilde{V}(\tilde{t})}{2} \right) \right] \frac{d\tilde{V}(\tilde{t})}{d\tilde{t}} = -\frac{\partial \tilde{c}^{(1)}}{\partial \tilde{x}}, \quad \alpha \left[\beta \sinh \left(\frac{\tilde{V}(\tilde{t})}{2} \right) - \cosh \left(\frac{\tilde{V}(\tilde{t})}{2} \right) \right] \frac{d\tilde{V}(\tilde{t})}{d\tilde{t}} = -\frac{\partial \tilde{\phi}^{(1)}}{\partial \tilde{x}}.$$
(34)

A similar evaluation of the time derivatives at the left electrode gives the effective boundary conditions at $\tilde{x}=-1$,

$$\alpha \left[\sinh \left(\frac{\tilde{V}(\tilde{t})}{2} \right) + \beta \cosh \left(\frac{\tilde{V}(\tilde{t})}{2} \right) \right] \frac{d\tilde{V}(\tilde{t})}{d\tilde{t}} = \frac{\partial \tilde{c}^{(1)}}{\partial \tilde{x}}, \quad \alpha \left[\beta \sinh \left(\frac{\tilde{V}(\tilde{t})}{2} \right) + \cosh \left(\frac{\tilde{V}(\tilde{t})}{2} \right) \right] \frac{d\tilde{V}(\tilde{t})}{d\tilde{t}} = \frac{\partial \tilde{\phi}^{(1)}}{\partial \tilde{x}}. \tag{35}$$

Equations (28) with the boundary conditions (34) and (35) form the $\mathcal{O}(\epsilon)$ problem. The applied voltage is oscillating, thus, we express the solutions as Fourier series, written in exponential form as

$$\tilde{c}^{(1)} = \sum_{k=1}^{\infty} \left(\tilde{c}_k^{(1)} e^{\iota k \tilde{t}} + (\tilde{c}_k^{(1)})^* e^{-\iota k \tilde{t}} \right); \quad \tilde{\phi}^{(1)} = \sum_{k=1}^{\infty} \left(\tilde{\phi}_k^{(1)} e^{\iota k \tilde{t}} + (\tilde{\phi}_k^{(1)})^* e^{-\iota k \tilde{t}} \right). \tag{36}$$

Here, the notation $(.)^*$ represents a complex conjugate. We focus on obtaining solutions for k positive, taking conjugates when needed. The governing equations for each k become

$$\iota k\alpha \tilde{c}_k^{(1)} = \frac{\partial^2 \tilde{c}_k^{(1)}}{\partial \tilde{x}^2}, \quad \iota k\alpha \beta \tilde{c}_k^{(1)} = \frac{\partial^2 \tilde{\phi}_k^{(1)}}{\partial \tilde{x}^2}.$$
 (37)

Note that there is no steady component of the $\mathcal{O}(\epsilon)$ potential: that is, over a time period of the field oscillation, $\tilde{\phi}^{(1)}$ averages to zero. Practically, this means that there cannot exist a time-averaged electric field at $\mathcal{O}(\epsilon)$. Hence, we seek the next higher order solution. The $\mathcal{O}(\epsilon^2)$ governing equations follow as

$$\alpha \frac{\partial \tilde{c}^{(2)}}{\partial \tilde{t}} = \frac{\partial^2 \tilde{c}^{(2)}}{\partial \tilde{x}^2}, \quad \alpha \beta \frac{\partial \tilde{c}^{(2)}}{\partial \tilde{t}} = \frac{\partial^2 \tilde{\phi}^{(2)}}{\partial \tilde{x}^2} + \frac{\partial}{\partial \tilde{x}} \left(\tilde{c}^{(1)} \frac{\partial \tilde{\phi}^{(1)}}{\partial \tilde{x}} \right). \tag{38}$$

Note that if $\tilde{\phi}^{(0)} \neq 0$, as discussed below, there would be a non-zero charge density at $\mathcal{O}(\epsilon^2)$ satisfying the corresponding Poisson equation, $\partial^2 \tilde{\phi}^{(0)}/\partial \tilde{x}^2 = \tilde{\rho}^{(2)}$. Consider the forcing term $\tilde{c}^{(1)} \frac{\partial \tilde{\phi}^{(1)}}{\partial \tilde{x}}$ in (38). This is a product of two infinite series of functions oscillating at integer harmonics. In general, this product would have terms that oscillate with frequencies which can be expressed as $(\pm k \pm j)$, where each k and j range from 1 to ∞ . The product of oscillators at k and -k lead to terms that are non-oscillating, or "steady." These steady terms result in an asymmetric rectified electric field, or "AREF," in the bulk of the cell. To proceed, we need to consider only the governing equation for the steady potential

$$0 = \frac{\partial^2 \tilde{\phi}_0^{(2)}}{\partial \tilde{x}^2} + \sum_{k=1}^{\infty} \frac{\partial}{\partial \tilde{x}} \left(\tilde{c}_k^{(1)} \frac{\partial (\tilde{\phi}_k^{(1)})^*}{\partial \tilde{x}} + (\tilde{c}_k^{(1)})^* \frac{\partial \tilde{\phi}_k^{(1)}}{\partial \tilde{x}} \right), \tag{39}$$

where the subscript '0' indicates a steady variable. The corresponding steady effective boundary conditions for the potential at $\tilde{x} = \pm 1$ are

$$0 = \frac{\partial \tilde{\phi}_0^{(2)}}{\partial \tilde{x}} + \sum_{k=1}^{\infty} \left(\tilde{c}_k^{(1)} \frac{\partial (\tilde{\phi}_k^{(1)})^*}{\partial \tilde{x}} + (\tilde{c}_k^{(1)})^* \frac{\partial \tilde{\phi}_k^{(1)}}{\partial \tilde{x}} \right). \tag{40}$$

Thus we have a system of equations, namely (39) and (40), that can be solved to examine the AREF, which is evidently $\mathcal{O}(\epsilon^2)$ at leading order in ϵ for frequencies on the bulk diffusion time. Finally, we remark that this formulation is valid until the applied voltage becomes "logarithmically large" [48, 49]. Specifically, we have implicitly assumed that the temporal variation in the leading order salt uptake in the $\mathcal{O}(\epsilon)$ wide Debye layers is small compared to unity. However, since $\tilde{I}_l^{(0)} = \tilde{I}_l^{(0)} = 4 \sinh^2 \left(\tilde{V}(\tilde{t})/4 \right)$ we see that the uptake can be of $\mathcal{O}(1)$ when $\epsilon \tilde{I}_r^{(0)} = \mathcal{O}(1)$, which translates to the dimensional criterion $V_0 = \mathcal{O}((2k_BT/e)\ln(1/(4\epsilon)))$. Thus, to proceed beyond the present analysis the leading order effective boundary conditions (27) will have to include the dynamics of salt uptake by the Debye layers. Consequently, the leading order ionic strength $\tilde{\epsilon}^{(0)}$ and potential $\tilde{\phi}^{(0)}$ will no longer be constants, and there will be a non zero charge density $\tilde{\rho}^{(2)}$ at $\mathcal{O}(\epsilon^2)$. The required analysis may necessitate the introduction of temporal boundary layers within the oscillation cycle, since even if $V_0 \gg (2k_BT/e)\ln(1/(4\epsilon))$ from $\tilde{I}_r^{(0)}$ we see that the rate of instantaneous salt uptake by the Debye layer is small at moments around when $d\tilde{V}(\tilde{t})/d\tilde{t}$ vanishes. We leave this to future work.

3 Results and discussion

The solution of (37) for the ionic strength is

$$\tilde{c}_k^{(1)} = A_k \sinh\left(m_k \tilde{x}\right) + B_k \cosh\left(m_k \tilde{x}\right),
\Longrightarrow \tilde{c}^{(1)} = \sum_{k=1}^{\infty} \left(\left(A_k \sinh\left(m_k \tilde{x}\right) + B_k \cosh\left(m_k \tilde{x}\right) \right) e^{\iota k \tilde{t}} + \left(A_k^* \sinh\left(m_k^* \tilde{x}\right) + B_k^* \cosh\left(m_k^* \tilde{x}\right) \right) e^{-\iota k \tilde{t}} \right);$$
(41)

and the potential is

$$\tilde{\phi}_{k}^{(1)} = \beta A_{k} \sinh (m_{k}\tilde{x}) + \beta B_{k} \cosh (m_{k}\tilde{x}) + L_{k}\tilde{x} + J_{k},$$

$$\implies \tilde{\phi}^{(1)} = \sum_{k=1}^{\infty} \left[\left(\beta A_{k} \sinh (m_{k}\tilde{x}) + \beta B_{k} \cosh (m_{k}\tilde{x}) + L_{k}\tilde{x} + J_{k} \right) e^{\iota k\tilde{t}} + \left(\beta A_{k}^{*} \sinh (m_{k}^{*}\tilde{x}) + \beta B_{k}^{*} \cosh (m_{k}^{*}\tilde{x}) + L_{k}^{*}\tilde{x} + J_{k}^{*} \right) e^{-\iota k\tilde{t}} \right].$$

$$(42)$$

Here $m_k^2 = \iota k \alpha$. From (34), taking only positive k, the effective boundary condition for the ionic strength at $\tilde{x} = 1$ becomes,

$$\alpha \left[\sinh \left(\frac{\tilde{V}(\tilde{t})}{2} \right) - \beta \cosh \left(\frac{\tilde{V}(\tilde{t})}{2} \right) \right] \frac{d\tilde{V}(\tilde{t})}{d\tilde{t}} = -\sum_{k=1}^{\infty} \left(A_k m_k \cosh \left(m_k \right) + B_k m_k \sinh \left(m_k \right) \right) e^{ik\tilde{t}}; \tag{43}$$

and the potential boundary condition is

$$\alpha \left[\beta \sinh \left(\frac{\tilde{V}(\tilde{t})}{2} \right) - \cosh \left(\frac{\tilde{V}(\tilde{t})}{2} \right) \right] \frac{d\tilde{V}(\tilde{t})}{d\tilde{t}} = -\sum_{k=1}^{\infty} \left(\beta A_k m_k \cosh \left(m_k \right) + \beta B_k m_k \sinh \left(m_k \right) + L_k \right) e^{ik\tilde{t}}. \tag{44}$$

Similarly from (35), at $\tilde{x} = -1$, the ionic strength boundary condition is

$$\alpha \left[\sinh \left(\frac{\tilde{V}(\tilde{t})}{2} \right) + \beta \cosh \left(\frac{\tilde{V}(\tilde{t})}{2} \right) \right] \frac{d\tilde{V}(\tilde{t})}{d\tilde{t}} = \sum_{k=1}^{\infty} \left(A_k m_k \cosh \left(m_k \right) - B_k m_k \sinh \left(m_k \right) \right) e^{ik\tilde{t}}, \tag{45}$$

and the potential boundary condition is

$$\alpha \left[\beta \sinh \left(\frac{\tilde{V}(\tilde{t})}{2} \right) + \cosh \left(\frac{\tilde{V}(\tilde{t})}{2} \right) \right] \frac{d\tilde{V}(\tilde{t})}{d\tilde{t}} = \sum_{k=1}^{\infty} \left(\beta A_k m_k \cosh \left(m_k \right) - \beta B_k m_k \sinh (m_k) + L_k \right) e^{ik\tilde{t}}. \tag{46}$$

Using the orthogonality of complex exponential functions on the sum and difference of (43) and (45); and substituting $\tilde{V}(\tilde{t}) = \nu \cos(\tilde{t})$, and $d\tilde{V}(\tilde{t})/d\tilde{t} = -\nu \sin(\tilde{t})$, where $\nu = V_0 e/(k_B T)$, we have

$$A_{k} = -\frac{\alpha\beta\nu\operatorname{sech}(m_{k})}{2\pi m_{k}} \int_{0}^{2\pi} \sin\left(\tilde{t}\right) \left[\cosh\left(\frac{\nu\cos(\tilde{t})}{2}\right)\right] e^{-\iota k\tilde{t}} d\tilde{t},\tag{47}$$

and

$$B_k = \frac{\alpha \nu \operatorname{csch}(m_k)}{2\pi m_k} \int_0^{2\pi} \sin\left(\tilde{t}\right) \left[\sinh\left(\frac{\nu \cos(\tilde{t})}{2}\right) \right] e^{-\iota k\tilde{t}} d\tilde{t}. \tag{48}$$

To find L_k , we use the linear combination (44) $-\beta$ (43), along with the orthogonality constraint to get

$$L_k = \frac{\alpha(\beta^2 - 1)\nu}{2\pi} \int_0^{2\pi} \sin\left(\tilde{t}\right) \left[\cosh\left(\frac{\nu\cos(\tilde{t})}{2}\right) \right] e^{-\iota k\tilde{t}} d\tilde{t}. \tag{49}$$

It can be shown that for odd k, $B_k=0$; and for even k, $A_k=0$, and $L_k=0$. Finally, we require that the potential at the center of the cell vanishes; thus, $J_k=-\beta B_k$. Hence we have

$$\tilde{c}^{(1)} = \begin{cases} \sum_{k=1}^{\infty} \left((A_k \sinh(m_k \tilde{x})) e^{\iota k \tilde{t}} + (A_k^* \sinh(m_k^* \tilde{x})) e^{-\iota k \tilde{t}} \right), & k = \text{odd}, \\ \sum_{k=1}^{\infty} \left((B_k \cosh(m_k \tilde{x})) e^{\iota k \tilde{t}} + (B_k^* \cosh(m_k^* \tilde{x})) e^{-\iota k \tilde{t}} \right), & k = \text{even}; \end{cases}$$

$$\tilde{\phi}^{(1)} = \begin{cases} \sum_{k=1}^{\infty} \left((\beta A_k \sinh(m_k \tilde{x}) + L_k \tilde{x}) e^{\iota k \tilde{t}} + (\beta A_k^* \sinh(m_k^* \tilde{x}) + L_k^* \tilde{x}) e^{-\iota k \tilde{t}} \right), & k = \text{odd}, \\ \sum_{k=1}^{\infty} \beta \left((B_k \cosh(m_k \tilde{x}) - B_k) e^{\iota k \tilde{t}} + (B_k^* \cosh(m_k^* \tilde{x}) - B_k^*) e^{-\iota k \tilde{t}} \right), & k = \text{even}. \end{cases}$$

$$(50)$$

Note that the even harmonics of the potential would disappear when the ions are symmetric, that is, $\beta = 0$. Thus we have the $\mathcal{O}(\epsilon)$ solution in the bulk. We can now calculate the AREF. Integrating (39) once gives,

$$-\frac{\partial \tilde{\phi}_0^{(2)}}{\partial \tilde{x}} = \sum_{k=1}^{\infty} \left(\tilde{c}_k^{(1)} \frac{\partial (\tilde{\phi}_k^{(1)})^*}{\partial \tilde{x}} + (\tilde{c}_k^{(1)})^* \frac{\partial \tilde{\phi}_k^{(1)}}{\partial \tilde{x}} \right) + L_0.$$
 (51)

From the boundary condition (40), we have $L_0 = 0$. From the $\mathcal{O}(\epsilon)$ solution (50), we have

$$\tilde{c}_{k}^{(1)} \frac{\partial (\tilde{\phi}_{k}^{(1)})^{*}}{\partial \tilde{x}} = \begin{cases} \beta A_{k} A_{k}^{*} m_{k}^{*} \sinh \left(m_{k} \tilde{x}\right) \cosh \left(m_{k}^{*} \tilde{x}\right) + A_{k} L_{k}^{*} \sinh \left(m_{k} \tilde{x}\right), & k = \text{odd}, \\ \beta B_{k} B_{k}^{*} m_{k}^{*} \cosh \left(m_{k} \tilde{x}\right) \sinh \left(m_{k}^{*} \tilde{x}\right), & k = \text{even}. \end{cases}$$

$$(52)$$

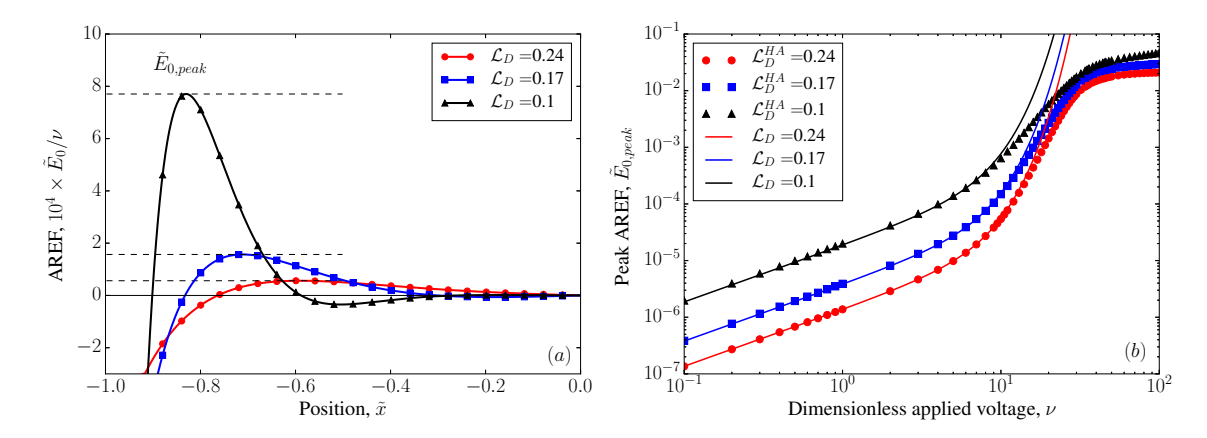


Fig. 2 (a) The AREF, re-normalized by ν , as a function of position in the left half cell for characteristic length scales, $\mathcal{L}_D=0.24,0.17,0.1;$ corresponding to $\alpha\approx32,62,181$. The horizontal dashed lines indicate the peak magnitudes of the AREF. (b) The peak values of the renormalized AREF as a function of the applied voltage, using our theory (solid lines) as compared to numerics by Hashemi Aremi et. al. [22] (symbols) for three values of \mathcal{L}_D . Here, $\kappa L=1300$ and $\beta=0.5$.

The AREF is then

$$\tilde{E}_0(\tilde{x}) \equiv -\epsilon^2 \frac{\partial \tilde{\phi}_0^{(2)}}{\partial \tilde{x}} = \epsilon^2 \left(f(\tilde{x}) + f^*(\tilde{x}) \right), \tag{53}$$

where

$$f(\tilde{x}) = \begin{cases} \sum_{k=1}^{\infty} \beta A_k A_k^* m_k^* \sinh(m_k \tilde{x}) \cosh(m_k^* \tilde{x}) + A_k L_k^* \sinh(m_k \tilde{x}), & k = \text{odd} \\ \sum_{k=1}^{\infty} (\beta B_k B_k^* m_k^* \cosh(m_k \tilde{x}) \sinh(m_k^* \tilde{x})), & k = \text{even.} \end{cases}$$

$$(54)$$

The values of A_k , B_k , and L_k (47) – (49) are found via numerical integration. We truncate the infinite sums in (50) and (53) at a sufficiently large value of $k=k_{max}$, which is determined by requiring that the relative error in the AREF calculated using two consecutive values of k_{max} is below a set tolerance. Typically, $k_{max}=10$ is chosen in the results that follow. Note, since the integrands in (47) – (49) are periodic in the interval $[0,2\pi]$, the value of the integral is exponentially small for large k (as can readily be shown via repeated integration by parts), thus the most significant contributions to the AREF come from the smaller values of k. Finally, in the limit of weak applied voltages, we can linearize the integrands in (47) – (49) to obtain the leading order AREF. We pursue the weak voltage limit in Sec. 3.1. Note that (53) is strictly valid in the bulk electrolyte, i.e., at a distance much larger than ϵ from the electrodes. However, this covers the range of practical interest, when considering the impact of AREFs on particle motion, for instance.

The AREF, \tilde{E}_0 , is an odd function of \tilde{x} , and is zero at the center of the cell. The AREF has a peak in magnitude, whose position depends on the applied frequency. From (53), a (dimensional) characteristic length scale, or range, of the AREF is obtained as $L/|m_1| = L/\sqrt{\alpha} = \sqrt{D_A/\omega}$. Thus, we see the inverse square root dependence of the range of the AREF as reported by previous authors in various instances of transiently perturbed Debye layers [22, 23, 45–47]. We use Fig. 2 to quantitatively compare our theory to the numerical observations by Hashemi Amrei et. al. (Fig. 5 in Ref. [22]). Therefore, we re-scale our theory to reflect the scaling used by those authors. Specifically, the AREF in the present work is normalized using a thermal voltage scale $k_BT/(Le)$, whereas Ref. [22] uses the applied voltage based scale V_0/L . Hence, we re-scale the AREF derived here by $V = V_0 e/(k_BT)$ to reflect this difference. That is, we plot \tilde{E}_0/ν on the y- axis in Fig 2. Further, α relates to the dimensionless distance \mathcal{L}_D , as defined by Ref. [22] and used in the plots, as

$$\mathcal{L}_D^2 = \frac{\pi}{4\alpha\sqrt{1-\beta^2}}. (55$$

Fig. 2 (a) illustrates the dependence of AREF on the frequency α , or equivalently, on \mathcal{L}_D , emphasizing the AREF peak magnitudes $\tilde{E}_{0,peak}$ at the different values of \mathcal{L}_D . Fig. 2 (b) shows the variation of $\tilde{E}_{0,peak}$ as a function of the applied voltage, as obtained by our theory (lines) and data from numerical observations (symbols) by Ref. [22]. The theory developed here matches well to the numerics at sufficiently small voltages, as expected. We see a linear response at weak voltages $\nu \ll 1$ and a transition to a nonlinear response at $\nu = \mathcal{O}(1)$. Our theory is expected to break down at logarithmically large voltages, which at $\epsilon = 1/(\kappa L) = 1/1300$ corresponds to $\nu \approx 12$. The breakdown of our theory is also demonstrated in Fig. 2 (b), as the theory indeed deviates from the numerical data at around $\nu = 12$.

We also make additional direct comparisons to results presented by Hashemi Amrei et. al. [22]. In this regard, we calculate the dependence of the magnitude of $\tilde{E}_{0,peak}$ on the dimensionless frequency α , or equivalently, \mathcal{L}_D . For

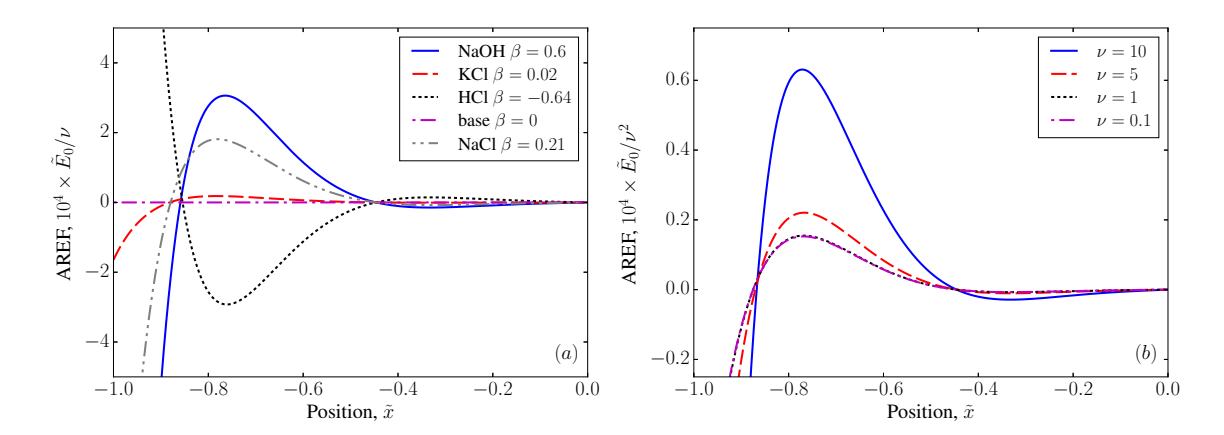


Fig. 3 The AREF as a function of the position in the left half cell (a) for different values of ion diffusivities for common electrolytes [31], for $\nu=10$; and (b) for applied voltages ranging from weak to moderate values, when $\beta=0.5$. Here, $\kappa L=1300$, and $\alpha=100$

this, note that $m_k \sim \mathcal{O}(\sqrt{\alpha})$; $A_k, B_k \sim \mathcal{O}(\alpha/m_k) = \mathcal{O}(\sqrt{\alpha})$; and $L_k \sim \mathcal{O}(\alpha)$. Thus, $A_k A_k^* m_k^*$, $B_k B_k^* m_k^*$, and $A_k L_k^* \sim \mathcal{O}(\alpha^{3/2})$. Thus, the peak AREF $\tilde{E}_{0,peak} \sim \mathcal{O}(\alpha^{3/2})$. Using (55), we have $\tilde{E}_{0,peak} \sim \mathcal{O}(\mathcal{L}_D^{-3})$. This scaling is demonstrated by Fig. 6 in Ref. [22]. Next, from (53), the AREF $\tilde{E}_0 \sim \mathcal{O}(\epsilon^2)$. This matches exactly to prediction from the full numerical simulations, as shown by Fig. 8 in Ref. [22].

The AREF is proportional to the difference in ionic diffusivities $\beta=(D_--D_+)/(D_-+D_+)$, and hence vanishes when the ions have equal diffusivities, $\beta=0$. Fig. 3 (a) shows the variation of the AREF with electrolyte type, represented by changing β . Note, $-1<\beta<1$. Due to the anti-symmetry of \tilde{E}_0 (53) about $\tilde{x}=0$, the transformation $\beta\to-\beta$ gives a reflection about the x-axis. If either ion has a diffusivity that is much larger than the other, that is, $|\beta|\to 1$, the behavior of the AREF changes significantly. Specifically, the peak observed for $|\beta|-1=\mathcal{O}(1)$ vanishes, that is, the AREF is monotonic. This can be understood mathematically as the coefficients $L_k\to 0$ for $|\beta|\to 1$, thus making the AREF purely a monotonic function. However, typical electrolytes have diffusivity ratios of $\mathcal{O}(1)$, hence the experimental observation of this limit may be difficult. Fig. 3 (a) is qualitatively similar to Fig. 8 in Ref. [34] who calculated the AREF using fully numerical as well as semi-analytical methods. Their semi-analytical solution is obtained by applying a weak voltage approximation to the full PNP equations; that is, without considering the thin Debye layer limit. They then solve the $\mathcal{O}(\nu^2)$ equations numerically, thereby obtaining a numerical evaluation of the weak-voltage AREF. Equation (53), and its weak voltage approximations to the AREF.

Fig. 3 (b) shows the AREF in the left half cell for different applied voltages. Here, the AREF is normalized by the square of the dimensionless applied voltage ν^2 to show the significance of higher order effects at moderately large voltages. At low voltages, the lines overlap, demonstrating that the leading order AREF is indeed $\mathcal{O}(\nu^2)$ in this limit. Thus our analysis provides a general analytic formulation of the AREF in the bulk of an electrochemical cell under a moderately large, oscillating voltage.

3.1 Weak voltage limit

We now consider the limit when the applied voltage is small compared to the thermal voltage. Formally, the weak voltage limit is defined as $\nu \ll 1$. In this limit, we expect the leading order contributions to the ionic strength and potential to come from the lowest harmonics. The leading order coefficients can be found by linearizing the expressions for A_1 and L_1 , since $B_1=0$. We use the expansion

$$\cosh\left(\frac{\nu\cos(\tilde{t})}{2}\right) = 1 + \frac{1}{2}\frac{\nu^2}{4}\cos^2(\tilde{t}) + \mathcal{O}(\nu^4) = 1 + \frac{\nu^2}{32}\left(e^{2\iota\tilde{t}} + e^{-2\iota\tilde{t}} + 2\right) + \mathcal{O}(\nu^4). \tag{56}$$

Here, we represented $\cos(\tilde{t}) = (e^{\iota \tilde{t}} + e^{-\iota \tilde{t}})/2$. Further using $\sin(\tilde{t}) = -\iota(e^{\iota \tilde{t}} - e^{-\iota \tilde{t}})/2$, we have from (47),

$$A_{1} = \frac{\iota \alpha \beta \operatorname{sech}(m_{1})}{4\pi m_{1}} \int_{0}^{2\pi} \left[\nu \left(1 - e^{-2\iota \tilde{t}} \right) + \frac{\nu^{3}}{32} \left(e^{2\iota \tilde{t}} + 1 - e^{-4\iota \tilde{t}} - e^{-2\iota \tilde{t}} \right) \right] d\tilde{t} + \mathcal{O}(\nu^{5}). \tag{57}$$

Since the integration is over a time period, all the oscillating (time-dependent) terms integrate out to zero. Thus we have

$$A_1 = \nu A_{11} + \mathcal{O}(\nu^3); \quad A_{11} = \frac{\iota \alpha \beta \operatorname{sech}(m_1)}{2m_1}.$$
 (58)

Note that A_1 (and A_1^*) are the only coefficients that have terms of $\mathcal{O}(\nu)$; all other A_k have higher order contributions in ν . Similarly, we calculate L_1 , which would contain the leading order contribution at the low voltage limit to get

$$L_1 = \nu L_{11} + \mathcal{O}(\nu^3); \quad L_{11} = \frac{\iota \alpha (1 - \beta^2)}{2}.$$
 (59)

The $\mathcal{O}(\epsilon)$ ionic strength and potential in the low voltage limit are thus

$$\tilde{c}_{1}^{(1)} = \nu A_{11} \sinh(m_{1}\tilde{x}) + \mathcal{O}(\nu^{3}); \quad \tilde{\phi}_{1}^{(1)} = \nu \left(\beta A_{11} \sinh(m_{1}\tilde{x}) + L_{11}\tilde{x}\right) + \mathcal{O}(\nu^{3}). \tag{60}$$

The leading order AREF is driven by the product $\tilde{c}_1^{(1)} \frac{\partial (\tilde{\phi}_1^{(1)})^*}{\partial \tilde{x}}$ and its conjugate. From (60),

$$\tilde{c}_{1}^{(1)} \frac{\partial (\tilde{\phi}_{1}^{(1)})^{*}}{\partial \tilde{x}} = \nu^{2} \left[\beta A_{11} A_{11}^{*} m_{1}^{*} \sinh (m_{1} \tilde{x}) \cosh (m_{1}^{*} \tilde{x}) + A_{11} L_{11}^{*} \sinh (m_{1} \tilde{x}) \right] + \mathcal{O}(\nu^{4}). \tag{61}$$

The leading order AREF is thus

$$\tilde{E}_{0} = \epsilon^{2} \nu^{2} \left[\beta A_{11} A_{11}^{*} m_{1}^{*} \sinh \left(m_{1} \tilde{x} \right) \cosh \left(m_{1}^{*} \tilde{x} \right) + A_{11} L_{11}^{*} \sinh \left(m_{1} \tilde{x} \right) \right. \\ \left. + \beta A_{11} A_{11}^{*} m_{1} \sinh \left(m_{1}^{*} \tilde{x} \right) \cosh \left(m_{1} \tilde{x} \right) + A_{11}^{*} L_{11} \sinh \left(m_{1}^{*} \tilde{x} \right) \right] + \mathcal{O}(\nu^{4}),$$
(62)

where the coefficients are given by (58) and (59). Thus the AREF $\tilde{E}_0 \sim \mathcal{O}(\epsilon^2 \nu^2)$ to leading order in the simultaneous limit of thin Debye layers and weak voltage. Note that the scaling of the AREF with ϵ and α (or \mathcal{L}_D) are explicitly captured even by the weak voltage analysis, and compares well to the numerical results of Ref. [22].

4 Particle motion under AREFs

We now consider the effect of the AREF on the time-averaged, or rectified, motion of a charged, dielectric, spherical particle. Particle motion under oscillating electric fields are of interest in colloidal assembly, where, for instance, a large number of such particles form planar structures above electrodes when subject to an ac voltage [13, 35]. The experimentally observed "height bifurcation" of colloidal particles in such experiments was attributed in recent work to the particle motion generated by the AREF, in addition to electro-hydrodynamic flow [22, 28]. Here, we recognize that in addition to the rectified electric field, we also have a transient concentration gradient in the bulk. Further, the AREF is nonuniform in space. Thus, a charged particle will move under the combined effects of electrophoresis and diffusiophoresis, and even an uncharged particle could move due to dielectrophoresis, in principle. Here we consider a particle which has a zeta potential $\zeta_p = \mathcal{O}(k_B T/e)$, where the subscript "p" is for particle. We expect classical models for electrophoresis [50] and diffusiophoresis [37] to hold in this regime. Further, we assume that for a particle at any given point \tilde{x}_p in the cell, the electric field $E(\tilde{x}_p)$ can be treated as the field at "infinity." This assumption also extends to concentration gradients that are functions of \tilde{x} . This is a reasonable first assumption in the bulk electrolyte when the particle radius is much smaller than the half-length of the cell; that is, over the size of the particle, the field and concentration do not change considerably.

The electrophoretic particle velocity is obtained using Smoluchowski's theory for a charged dielectric particle with a thin Debye layer, $U_{EP} = M_{EP} E(\tilde{x}_p)$, where $M_{EP} = \varepsilon \zeta_p/\eta$, and η is the viscosity of the electrolyte solution. The velocity is linear in the electric field, hence the averaged electrophoretic velocity is obtained by replacing the electric field with its time-averaged value, which up to moderate voltages is given by the AREF (53). Further, in our one dimensional system, the electric field, and hence the velocity, are in the direction perpendicular to the electrodes, hence we only consider their magnitudes hereafter. The magnitude of the (dimensional) rectified electrophoretic velocity is

$$\langle U_{EP} \rangle = \frac{\varepsilon \zeta_p}{\eta} \left(\frac{k_B T}{Le} \right) \left[\tilde{E}_0 + \mathcal{O} \left(\epsilon^4 \right) \right] \sim \left(\frac{\varepsilon k_B^2 T^2}{e^2 \eta L} \right) \tilde{\zeta}_p \tilde{E}_0. \tag{63}$$

Here, the angular brackets $\langle . \rangle$ indicate a time-average, $\tilde{\zeta}_p$ is a dimensionless particle zeta potential normalized by the thermal voltage, and we have used $k_BT/(Le)$ as the normalization of electric field. Notice that $\varepsilon k_B^2T^2/(e^2\eta L)$ emerges as the scale of the electrophoretic velocity. Using (53) in (63), we calculate the electrophoretic velocity as a function of the position \tilde{x}_p . Since the electrophoretic mobility is constant in space, the roots of the AREF are the roots of the electrophoretic velocity. Thus, a charged particle at the center of the cell will not experience net electrophoretic motion. Physically, the roots of the AREF are positions away from the center of the cell where the particle would undergo no net electrophoretic motion. However, only some roots are "stable," and hence practically observable. Consider a positively charged particle ($\tilde{\zeta}_p > 0$) in an electrolyte with $\beta > 0$, in the left half-cell ($\tilde{x}_p < 0$). The dimensionless, rectified electrophoretic velocity of such a particle, that is, from (63), $\langle \tilde{U}_{EP} \rangle = \tilde{\zeta}_p \tilde{E}_0$, is shown in Fig. 4 (a) by the dashed red curve. Here, the second root in the left half of the cell would behave as a stable position. This is understood physically by

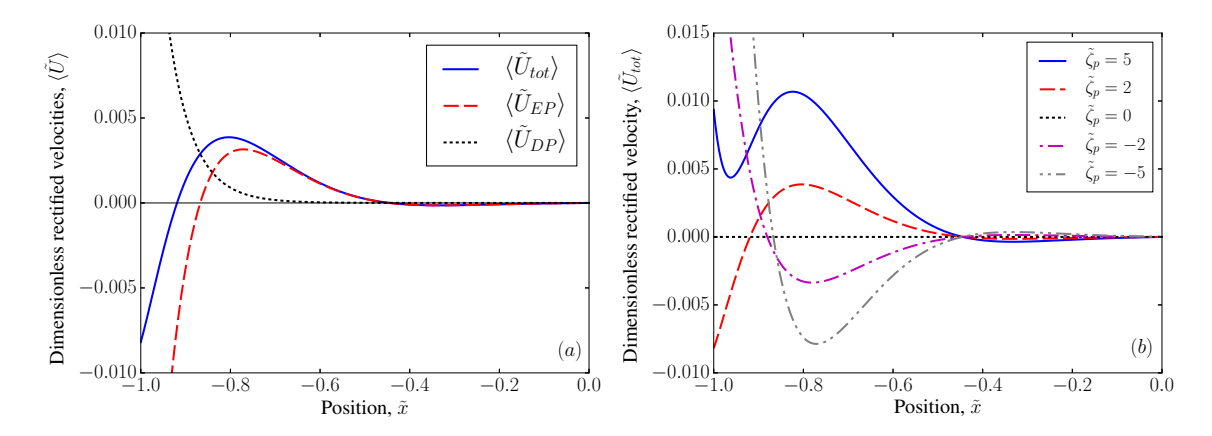


Fig. 4 The dimensionless, rectified velocity (of $\mathcal{O}(\epsilon^2)$), normalized by $\varepsilon k_B^2 T^2/(e^2 \eta L)$, of a charged dielectric spherical particle. (a) The electrophoretic and diffusiophoretic contributions to the total velocity for $\zeta_p = 2k_BT/e$. (b) The total velocity for a range of zeta potentials. Here, $\alpha = 100$, $\kappa L = 1300$ and $\beta = 0.5$, and $\nu = 10$.

considering the sign, or direction, of the AREF, or equivalently, the direction of electrophoretic velocity, for a positively charged particle on either side of the root. If the particle is perturbed slightly to the right of the stable root, the AREF here is negative, or to the left. Similarly, if the particle is perturbed to the left, the AREF is positive, or to the right. In either case, the particle would return to its initial position, hence, the root is considered stable. Conversely, under the same conditions, the first root in the left half cell is "unstable," i.e., a particle perturbed from this position will continue to move away from it. Notably, on the left of the first root, the particle continues to move leftward, hence approaching the Debye layer. An equivalent analysis can identify stable roots for $\beta < 0$, $\tilde{\zeta}_p < 0$, or $\tilde{x}_p > 0$. Mathematically, a stable root of the electrophoretic velocity is determined as a root where its gradient is negative [51]. For the one-dimensional system considered here, this condition becomes $\partial U_{EP}/\partial \tilde{x}_p < 0$. This result is also obtained in [22]. Here, we reiterate that the electrophoretic motion does not completely describe the behavior of a charged particle under an AREF, however.

The diffusiophoretic velocity is proportional to the logarithm of the normalized ionic strength gradient, $U_{DP} = M_{DP} \nabla \ln(c(\tilde{x}_p)/c_{eq})$, where M_{DP} is the diffusiophoretic mobility [37, 38]. The driving force for diffusiophoresis is inherently nonlinear in the ionic strength, thus we should expect a rectified diffusiophoretic velocity whenever there is a bulk ionic strength gradient, even if this gradient is transient. The driving force for diffusiophoresis $\nabla \ln(c/c_{eq}) = \nabla \ln(\tilde{c})$ is obtained from our asymptotic solution for \tilde{c} and by using a Taylor series expansion of $\ln(1+z)$, where z represents the total perturbation, of $\mathcal{O}(\epsilon)$ and higher, to the bulk ionic strength; that is,

$$\ln\left(\tilde{c}\right) = \left[\epsilon \tilde{c}^{(1)} + \epsilon^2 \tilde{c}^{(2)}\right] - \frac{1}{2} \left[\epsilon \tilde{c}^{(1)} + \epsilon^2 \tilde{c}^{(2)}\right]^2 + \mathcal{O}(\epsilon^5). \tag{64}$$

The rectified driving force is obtained by first taking the time-average and then calculating the gradient of (64). From (41), $\tilde{c}^{(1)}$ does not have steady, time-independent terms. Similarly, from (28), $\tilde{c}^{(2)}$ cannot have any steady, non-constant terms. Thus, the gradients of $\tilde{c}^{(1)}$ and $\tilde{c}^{(2)}$ average to zero over an oscillation cycle. The leading order driving force thus comes from $(\tilde{c}^{(1)})^2$. Here, the steady terms arise from products of oscillators at equal and opposite frequencies, +k and -k. From (50), we have the rectified driving force for diffusiophoresis,

$$\langle \nabla \ln \left(\tilde{c} \right) \rangle = -\epsilon^2 \sum_{k=1}^{\infty} \nabla \left(\tilde{c}_k^{(1)} (\tilde{c}_k^{(1)})^* \right) + \mathcal{O}(\epsilon^4). \tag{65}$$

Thus, the leading order driving force for diffusiophoresis under an ac voltage is obtained from the $\mathcal{O}(\epsilon)$ perturbation of the ionic strength. Further, note that the $\mathcal{O}(\epsilon^2)$ driving force has a negative sign, which is unlike diffusiophoresis in the linear regime [37, 38]. We obtain the magnitude of the rectified diffusiophoretic velocity (in our one-dimensional system) as

$$\langle U_{DP} \rangle = -M_{DP} \left[\epsilon^2 \sum_{k=1}^{\infty} \left(\tilde{c}_k^{(1)} \frac{\partial (\tilde{c}_k^{(1)})^*}{\partial \tilde{x}} + (\tilde{c}_k^{(1)})^* \frac{\partial \tilde{c}_k^{(1)}}{\partial \tilde{x}} \right) + \mathcal{O}(\epsilon^4) \right], \tag{66}$$

where

$$\tilde{c}_{k}^{(1)} \frac{\partial (\tilde{c}_{k}^{(1)})^{*}}{\partial \tilde{x}} = \begin{cases} A_{k} A_{k}^{*} m_{k}^{*} \sinh \left(m_{k} \tilde{x}\right) \cosh \left(m_{k}^{*} \tilde{x}\right), & k = \text{odd}, \\ B_{k} B_{k}^{*} m_{k}^{*} \cosh \left(m_{k} \tilde{x}\right) \sinh \left(m_{k}^{*} \tilde{x}\right), & k = \text{even}; \end{cases}$$

$$(67)$$

and the diffusiophoretic mobility is [37]

$$M_{DP} = \left(\frac{\varepsilon k_B^2 T^2}{e^2 \eta L}\right) \left[\beta \tilde{\zeta}_p + 4 \ln \left(\cosh \left(\frac{\tilde{\zeta}_p}{4}\right)\right)\right]. \tag{68}$$

Note that the diffusiophoretic velocity follows the same scaling as the electrophoretic one; hence, we expect the two to be comparable in general. The diffusiophoretic mobility, and hence velocity, consists of two terms, the first is due to the electric field generated as a result of the concentration gradient. This term depends linearly on the zeta potential, and also on the difference in diffusivities β , since an electric field is generated in an electrolyte concentration gradient only when the ions have different diffusivities. Further, the direction of electric field depends on the sign of β , i.e., on which ion is faster. Note, to leading order in $\tilde{\zeta}_p$, the diffusiophoretic mobility scales as $\beta \tilde{\zeta}_p$. The second term describes the motion of a charged particle in an osmotic pressure gradient. This term depends non-linearly on the zeta potential and does not depend on the difference in diffusivities of the ions. The second term in M_{DP} is always positive, thus a particle under an ac voltage, on average, is driven up the concentration gradient. The first term, that may be positive or negative, can drive a particle either up or down the concentration gradient, on average. Thus, the rectified diffusiophoretic velocity could either be up or down the concentration gradient depending on the zeta potential ζ_p and the difference in the diffusivities β . When the product $\zeta_p\beta > 0$, the two terms in M_{DP} are additive. Thus the diffusiophoretic velocity becomes close in magnitude and opposite in sign to the electrophoretic velocity, and the total particle velocity deviates from the electrophoretic velocity. This is shown by the dotted black curve (diffusiophoretic velocity) and the solid blue curve (total particle velocity) in Fig. 4 (a). However, if the product $\zeta_p\beta < 0$, the two terms in M_{DP} have opposite effects, thus the total diffusiophoretic velocity is smaller than the electrophoretic velocity, and thus the electrophoretic velocity dominates the total rectified velocity.

Fig. 4 (b) shows how the zeta potential affects the total rectified velocity. When $\tilde{\zeta}_p < 0$ (dot-dashed magenta and dot-dot-dashed grey curves) the total velocity resembles the electrophoretic velocity. However, when $\tilde{\zeta}_p > 0$ (solid blue and dashed red curves) the total velocity deviates from pure electrophoresis. The position of the stable root does not change with zeta potential. This is expected as the root only depends on the characteristic length scale, and hence the frequency of input voltage. For certain zeta potentials, there is an unstable root that is different from that of the AREF, and for larger zeta potentials, the diffusiophoretic velocity is so large that there is no unstable root, thus the particle has only one equilibrium position in the left half cell. Clearly, then, one must consider rectified diffusiophoresis when attempting to accurately predict particle motion under an AREF.

Finally, we expect that an uncharged particle would also move under the AREF since it is spatially non-uniform. By a scaling analysis, we get that the dielectrophoretic mobility is a factor $(a/L)^2 \ll 1$ smaller than the electrophoretic and dielectrophoretic contributions. Hence, we neglect this contribution to the total particle velocity.

5 Conclusions

We have presented a thin double layer analysis of the asymmetric rectified electric field generated when an ac voltage is applied to a binary monovalent electrolyte with unequal ionic diffusivities. Accounting for unequal ionic diffusivities gives rise to a transient ionic strength gradient in the bulk electrolyte that causes a nonzero rectified electric potential at second order in the normalized Debye layer thickness. At frequencies comparable to the inverse bulk diffusion time scale, the range of the AREF emerges from our analysis (and also from numerical work in Ref. [22, 28]) as $\sqrt{D_A/\omega}$. The characteristic amplitude of the AREF is $\mathcal{O}(\epsilon^2\beta)$ for moderate voltages, and is $\mathcal{O}(\epsilon^2\nu^2\beta)$ for weak voltages to leading order. Further, we discuss the implications of an AREF to the motion of charged colloidal particles under an ac voltage. Notably, in addition to electrophoretic motion under the AREF, charged particles also undergo rectified diffusiophoresis due to the bulk ionic strength gradient. The existence of bulk ionic strength gradients that occur due to differences in ionic diffusivities should be expected as a norm, rather than an exception. We demonstrate the effect of these transient ionic strength gradients to the motion of a charged dielectric spherical particle. It would be interesting to study its effect on particle motion beyond the simple case considered here; for instance, conducting particles that would exhibit induced charge electrokinetics, or considering more than one particle.

The AREF is a general nonlinear phenomenon that occurs when any oscillating voltage, including non-sinusoidal signals, is applied across an asymmetric electrolyte between polarizable electrodes. It can be viewed as the electrochemical analog to "steady streaming," where a time-averaged, or rectified, velocity field is generated in the bulk (viscous) fluid due to the oscillation of an immersed particle [52]. In that case, there is a momentum diffusion boundary layer akin to the Debye layer in the present problem. The thin Debye layer analysis yields a set of equations (8), (22), and (24), that provide a macro-scale description of the bulk electrolyte from which the bulk AREF, which is of practical interest, can be calculated. These equations could be solved numerically at voltages beyond the logarithmically large voltage limit considered here. Additionally, one can go beyond our model one dimensional system to include the effects of the curvature or roughness of electrodes [43, 53] that would introduce a second (or third) spatial dimension for ion transport and fluid flow in the bulk. There, the effective boundary conditions (22) and (24) must be generalized to include ion fluxes tangential to the electrode surface, i.e., "surface conduction," along with the normal fluxes considered here.

Acknowledgements We acknowledge support from the National Science Foundation through Grant No. CBET-2002120, and the Toor Fellowship in Chemical Engineering, Carnegie Mellon University (B. B.). We thank the authors of [22] for sharing their data.

References

- 1. G. Barbero, I. Lelidis, Physical Review E **76**(5), 051501 (2007)
- 2. P.J. Beltramo, R. Roa, F. Carrique, E.M. Furst, Journal of colloid and interface science 408, 54 (2013)
- 3. A. Hollingsworth, D. Saville, Journal of colloid and interface science 257(1), 65 (2003)
- 4. S.S. Dukhin, Advances in colloid and interface science **35**, 173 (1991)
- 5. A. Ramos, H. Morgan, N.G. Green, A. Castellanos, Journal of colloid and interface science 217(2) (1999)
- 6. A. Ajdari, Physical Review E **61**(1), R45 (2000)
- 7. V. Studer, A. Pépin, Y. Chen, A. Ajdari, Analyst **129**(10), 944 (2004)
- 8. J. Catalano, P. Biesheuvel, EPL (Europhysics Letters) 123(5), 58006 (2018)
- 9. P. Biesheuvel, Y. Fu, M. Bazant, Russian Journal of Electrochemistry 48(6), 580 (2012)
- 10. A. Campione, L. Gurreri, M. Ciofalo, G. Micale, A. Tamburini, A. Cipollina, Desalination 434, 121 (2018)
- 11. S. Al-Amshawee, M.Y.B.M. Yunus, A.A.M. Azoddein, D.G. Hassell, I.H. Dakhil, H.A. Hasan, Chemical Engineering Journal 380, 122231 (2020)
- 12. D.C. Prieve, P.J. Sides, C.L. Wirth, Current Opinion in Colloid & Interface Science 15(3), 160 (2010)
- 13. J.D. Hoggard, P.J. Sides, D.C. Prieve, Langmuir **24**(7), 2977 (2008)
- 14. X. Yang, N. Wu, Langmuir 34(3), 952 (2018)
- 15. P.R. Gascoyne, J. Vykoukal, Electrophoresis **23**(13), 1973 (2002)
- 16. Q. Chen, Y.J. Yuan, RSC advances 9(9), 4963 (2019)
- 17. N. Abd Rahman, F. Ibrahim, B. Yafouz, Sensors 17(3), 449 (2017)
- 18. X. Chen, Y. Ren, W. Liu, X. Feng, Y. Jia, Y. Tao, H. Jiang, Analytical chemistry 89(17), 9583 (2017)
- 19. H.C. Chang, G. Jaffé, The Journal of Chemical Physics 20(7), 1071 (1952)
- 20. J.R. Macdonald, Physical review **92**(1), 4 (1953)
- 21. M.Z. Bazant, K. Thornton, A. Ajdari, Physical review E 70(2), 021506 (2004)
- 22. S.H. Amrei, G.H. Miller, W.D. Ristenpart, Physical Review E **99**(6), 062603 (2019)
- 23. L.H. Olesen, M.Z. Bazant, H. Bruus, Physical Review E 82(1), 011501 (2010)
- 24. O. Schnitzer, E. Yariv, Physical Review E **89**(3), 032302 (2014)
- 25. A.S. Khair, T.M. Squires, Physics of Fluids **20**(8), 087102 (2008)
- 26. R.F. Stout, A.S. Khair, Physical Review E **92**(3), 032305 (2015)
- 27. A. Bandopadhyay, V.A. Shaik, S. Chakraborty, Physical Review E 91(4), 042307 (2015)
- 28. S.H. Amrei, S.C. Bukosky, S.P. Rader, W.D. Ristenpart, G.H. Miller, Physical review letters 121(18), 185504 (2018)
- 29. F. Freire, G. Barbero, M. Scalerandi, Physical Review E 73(5), 051202 (2006)
- 30. J. Kim, S. Davidson, A. Mani, Micromachines **10**(3), 161 (2019)
- 31. P. Vanysek, CRC handbook of chemistry and physics 83, 76 (2000)
- 32. S.C. Bukosky, S. Hashemi Amrei, S.P. Rader, J. Mora, G.H. Miller, W.D. Ristenpart, Langmuir 35(21), 6971 (2019)
- 33. S.H. Amrei, G.H. Miller, W.D. Ristenpart, Physical Review Fluids 5(1), 013702 (2020)
- 34. S.H. Amrei, G.R. Miller, K.J. Bishop, W. Ristenpart, Soft Matter (2020)
- 35. S.C. Bukosky, W.D. Ristenpart, Langmuir 31(36), 9742 (2015)
- 36. C.L. Wirth, P.J. Sides, D.C. Prieve, Physical Review E **87**(3), 032302 (2013)
- 37. D. Prieve, J. Anderson, J. Ebel, M. Lowell, Journal of Fluid Mechanics 148, 247 (1984)
- 38. R.A. Rica, M.Z. Bazant, Physics of Fluids **22**(11), 112109 (2010)
- 39. B. Balu, A.S. Khair, Physical Review Research 2(1), 013138 (2020)
- 40. I. Rubinstein, B. Zaltzman, Mathematical Models and Methods in Applied Sciences 11(02), 263 (2001)
- 41. M.Z. Bazant, K.T. Chu, B.J. Bayly, SIAM journal on applied mathematics 65(5), 1463 (2005)
- 42. J. Newman, K.E. Thomas-Alyea, Electrochemical systems (John Wiley & Sons, 2012)
- 43. K.T. Chu, M.Z. Bazant, Physical Review E **74**(1), 011501 (2006)
- 44. E.H. DeLacey, L.R. White, Journal of the Chemical Society, Faraday Transactions 2: Molecular and Chemical Physics **78**(3), 457 (1982)
- 45. W.C. Chew, P. Sen, The Journal of chemical physics **77**(9), 4683 (1982)
- 46. A. Gonzalez, A. Ramos, P. García-Sánchez, A. Castellanos, Physical Review E **81**(1), 016320 (2010)
- 47. P. García-Sánchez, N.G. Loucaides, A. Ramos, Physical Review E 95(2), 022802 (2017)
- 48. O. Schnitzer, E. Yariv, Physical Review E **86**(6), 061506 (2012)
- 49. O. Schnitzer, E. Yariv, Physical Review E **86**(2), 021503 (2012)
- 50. D. Saville, Annual Review of Fluid Mechanics 9(1), 321 (1977)
- 51. S.H. Strogatz, Nonlinear dynamics and chaos with student solutions manual: With applications to physics, biology, chemistry, and engineering (CRC press, 2018)
- 52. N. Riley, The Quarterly Journal of Mechanics and Applied Mathematics 19(4), 461 (1966)
- 53. M. Janssen, Physical Review E **100**(4), 042602 (2019)